

PAPER • OPEN ACCESS

GANs enabled super-resolution reconstruction of wind field

To cite this article: Duy Tan Tran *et al* 2020 *J. Phys.: Conf. Ser.* **1669** 012029

View the [article online](#) for updates and enhancements.



IOP | ebooks™

Bringing together innovative digital publishing with leading authors from the global scientific community.

Start exploring the collection—download the first chapter of every title for free.

GANs enabled super-resolution reconstruction of wind field

Duy Tan Tran¹, Haakon Robinson¹, Adil Rasheed^{1,2}, Omer San³,
Mandar Tabib², Trond Kvamsdal^{2,4}

¹Department of Engineering Cybernetics, NTNU, Trondheim, Norway

²Mathematics and Cybernetics, SINTEF Digital, Trondheim, Norway

³School of Mechanical and Aerospace Engineering, OSU, Oklahoma, USA

⁴Department of Mathematical Sciences, NTNU, Trondheim, Norway

E-mail: haakon.robinson@ntnu.no, adil.rasheed@ntnu.no, osan@okstate.edu,
mandar.tabib@sintef.no, trond.kvamsdal@sintef.no

Abstract. Atmospheric flows are governed by a broad variety of spatio-temporal scales, thus making real-time numerical modeling of such turbulent flows in complex terrain at high resolution computationally unmanageable. In this paper, we demonstrate a novel approach to address this issue through a combination of fast coarse scale physics based simulator and a family of advanced machine learning algorithm called the Generative Adversarial Networks. The physics-based simulator generates a coarse wind field in a real wind farm and then ESRGANs enhance the result to a much finer resolution. The method outperforms state of the art bicubic interpolation methods commonly utilized for this purpose.

1. Introduction

Optimal wind turbine siting and power production forecasting in windfarms require accurate knowledge of local wind field. Generally, measurement campaigns are undertaken to obtain an insight into the prevailing wind conditions at a particular site. These campaigns are expensive, and yield very coarse resolution wind data. Numerical simulation is therefore, an attractive alternative to the measurement campaigns. However, high resolution numerical simulation is computationally intractable, in particular in the context of digital twins [1]. The current work addresses this issue through an innovative combination of traditional numerical solvers (computational fluid dynamics codes) and advanced machine learning algorithm called Generative Adversarial Networks (GANs). A traditional high fidelity numerical flow solver is used to generate a very coarse scale wind field, and then a pre-trained GANs is used to refine the resolution to be suitable for accurate aerodynamic simulations of the wind turbines [2].

In the subsequent sections, we give a brief high level understanding of the numerical solver and GANs followed by the description of the data and GANs setup. We then present some sample results which convincingly demonstrate the superiority of our approach against commonly used interpolation schemes such as bicubic interpolation.

2. Theory

The dataset used in this work was generated using a unidirectionally coupled HARMONIE-SIMRA multiscale system. HARMONIE [3] is a meteorological program used for weather



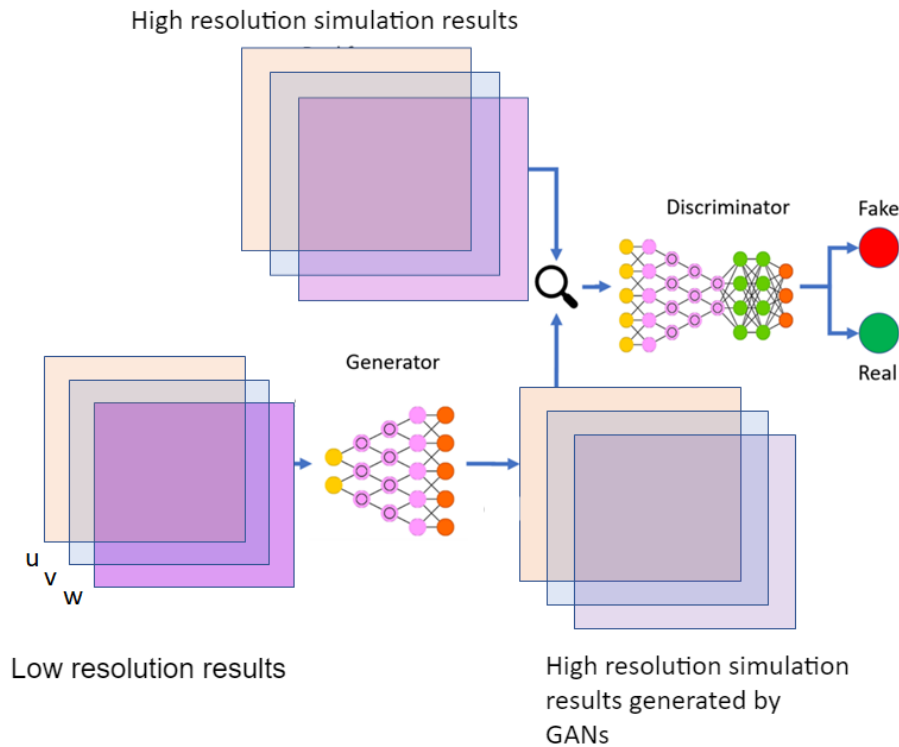


Figure 1. High-level block diagram of a GANs.

forecasting in Norway and SIMRA [4, 5] is a program specially designed to model terrain-induced wind and turbulence in complex terrain at high horizontal spatial resolution, and is capable of resolving important terrain features. Both these programs are based on the mass, momentum and energy conservation principles of fluid mechanics. More details regarding the use of the multiscale coupled HARMONIE-SIMRA for wind farm simulations can be found in [6, 7]. GANs are innovative models first conceived by Goodfellow in 2014 [8], where two deep neural networks, commonly called the generator and discriminator, are made to compete against each other. The generator takes noise (in this case the coarse scale wind field) and outputs a realistic synthetic example of its training set (the fine scale wind field). The discriminator then evaluates if the output generated by the generator appears realistic or fake. The two competing networks are trained simultaneously, each of them trying to outperform the other. The result is a generator network that can produce realistic outputs that lie within the training data distribution. Fig. 1 shows the structure of a typical GANs.

3. Data Generation

For the generation of data, HARMONIE-SIMRA coupled system was utilized. The HARMONIE was operated at a horizontal resolution of $2.5 \text{ km} \times 2.5 \text{ km}$ shown in Fig. 2(a) while SIMRA was operated at a resolution of $200 \text{ m} \times 200 \text{ m}$. The model has been in operation since 1st July 2017, generating an hourly stream of three dimensional wind field for a domain size of $30 \text{ km} \times 30 \text{ km} \times 3 \text{ km}$ corresponding to the one shown in Fig. 2(b). Due to the enormous amount of data and limits of the available computational infrastructure, we demonstrate our approach in a two dimensional setting only. The two dimensional horizontal planes were extracted from the raw data at 39m above the terrain and treated as the high resolution data we intend to generate using the GANs. The coarse scale data was obtained by downsampling this data to a

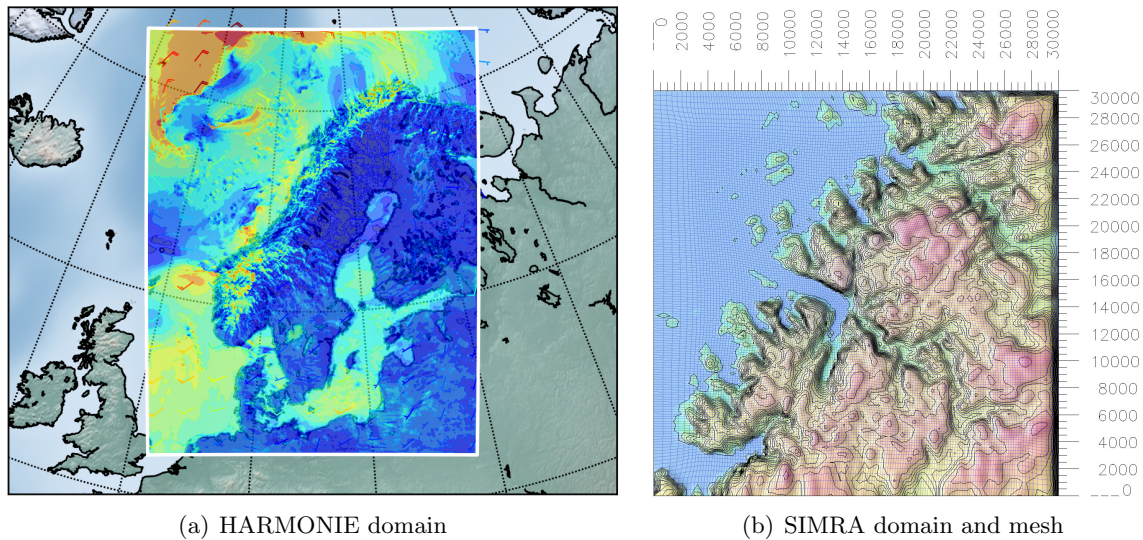


Figure 2. Domains of the HARMONIE and SIMRA simulators

coarser resolution using the nearest neighbor algorithm. This downsampled data will act as the input to the GANs network and the original fine scale data is treated as the target.

4. GANs setup

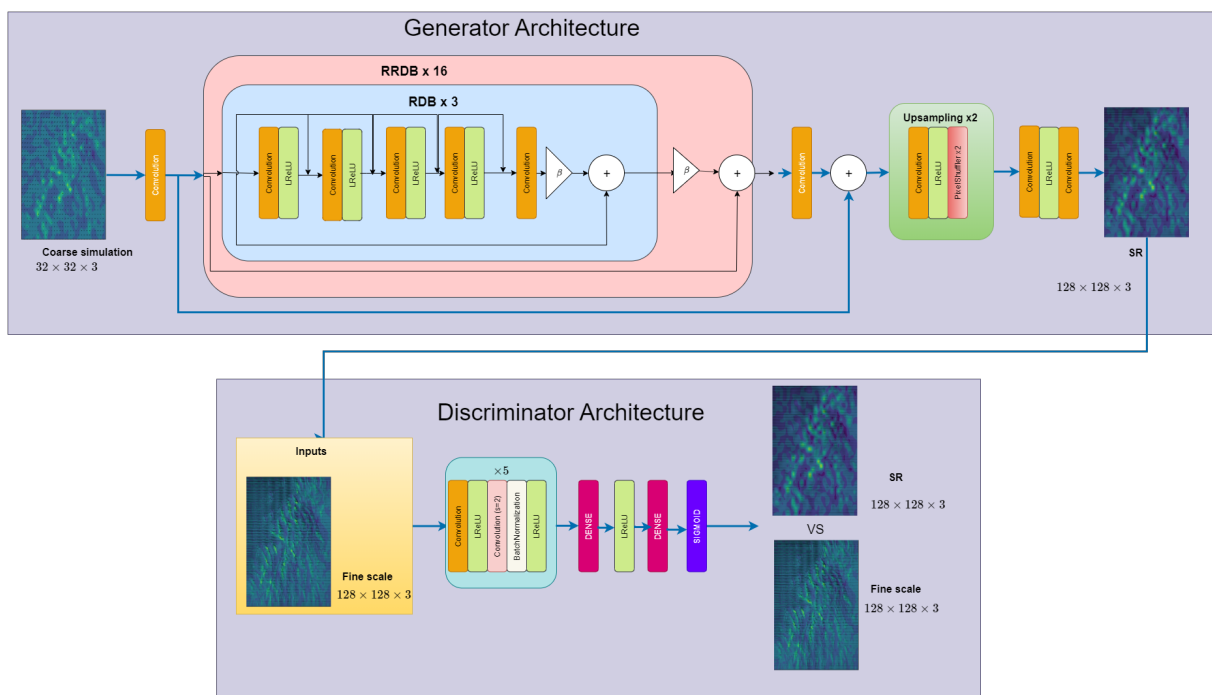
The exact architecture of the GANs model implemented and used in this project is inspired by the work presented in [11], the structure of which is shown in Fig. 3. The basic network unit is the Residual-in-Residual Dense Block (RRDB) without batch-normalization layers, shown as a red block in the figure. As a result of removing batch-normalization, the training becomes more stable with a consistent performance. After the last convolution layer, the residual features are multiplied locally by a factor of $\beta = 0.2$ for each residual block to proper fix the initialization, thus averting multiplying the input signals' magnitudes in the residual network. Furthermore, the generator network G in Fig. 3 consists of two convolutional layers with 5×5 kernels, and 128 feature maps with LeakyReLU as the activation function. At the end of the network, the resolution of the input image is increased through two sub-pixel convolution layers. The discriminator network in Fig. 3 uses LeakyReLU activation while avoiding max-pooling during the whole training period. It consists of five convolutional layers with an increasing number of 3×3 filter kernels, expanding by a factor of 2 from 64 to 512 kernels. For each time the number of features is doubled. Strided convolutions are applied for the image resolution reduction. As is common practice, zero-padding (i.e., padding the input volume with zeros) was utilized in order to control the output shape. At the end of the D network, the binary classification probability is computed by two dense layers and a final sigmoid activation function. Table 1 shows the tuned hyperparameters used in this work. The first parameter is self-explanatory, as we want to enhance the coarse simulation results by a factor of 4. We also tried to adjust the network architecture's depth, but from experience, GANs often earn more from having a wider network than deeper. However, a too wide model will result in GPU memory explosion. By increasing the number of filters (features), the sharpness of the generated images was more visually pleasing, but the number of parameters increased immensely. A useful tool applied was the local feature fusion with kernel size of 1 at the end of the residual dense block, which resulted in almost 50% reduction of the number of weights, and no change in the performance at all. Hence, the training phase was much faster. At last, 150k iterations yielded convergence.

For application of GANs in reconstruction of fluid flow, an effective loss function can be

Table 1. $\times 4$: Table of hyperparameters after fine tuning.

Parameter	Value
Scale	4
Base no. of Features (G)	128
Base no. of Features (D)	128
Kernel size (G)	5×5
Local Feature fusion (G)	1×1
No. of iterations	150k

difficult to design. The common loss function used for this is the MSE (Mean Squared Error) between the network output patch and the ground truth high-resolution patch. Here, we have used a perceptual loss function developed by Johnson [9]. In order to compute this loss function, the difference in feature map activations in high layers of a VGG network [10] between the network output patch and the high resolution patch is considered. The feature map activations are thus denoted as a perceptual loss metric.

**Figure 3.** Architecture of ESRGAN network.

5. Results and discussions

This section presents the performance of the trained network on new unseen data set. Fig. 4 gives a comparison of the GANs approach and bicubic interpolation with respect to the ground truth. In the figure, the wind field in the first column corresponds to the coarse resolution field subsampled from the high resolution field in the fourth column. Second column corresponds to the high resolution wind field obtained by applying bicubic interpolation on the subsampled wind field. The third column corresponds to the high resolution field obtained from the application of the trained GANs on the coarse field. It is very clear that the GANs is able to successfully construct the high resolution field consistently. For a quantitative evaluation, the peak signal to noise ratio ($PSNR$) is also presented in the figure. The $PSNR$ in the current context is defined via the mean squared error (MSE) computed from the original wind field and its noisy (bicubic or ESRGANs) approximations. Mathematically:

$$PSNR = 20 \cdot \log_{10}(MAX_1) - 10 \cdot \log_{10}(MSE) \quad (1)$$

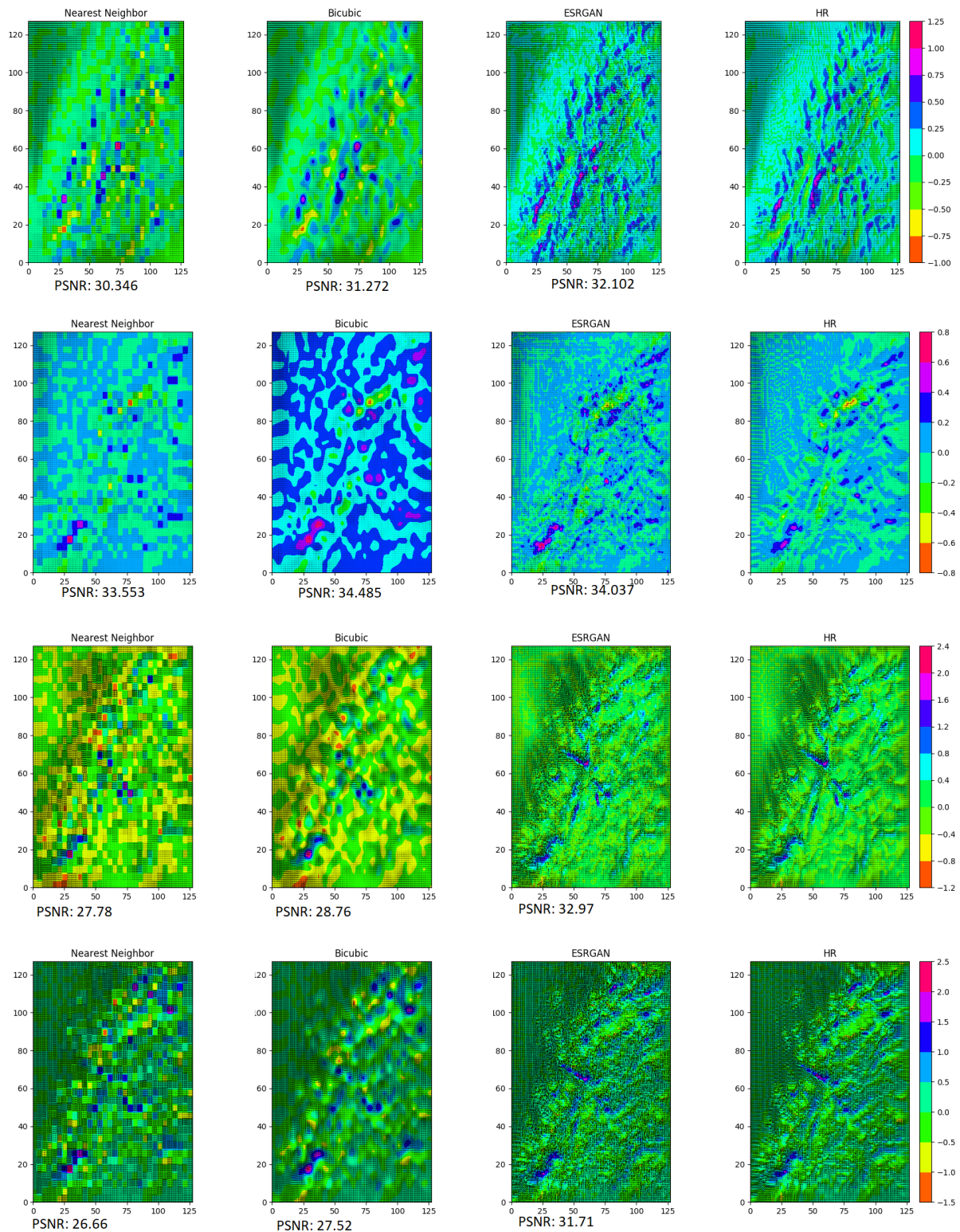


Figure 4. More $\times 4$ enhanced qualitative results (from left to right) of the nearest neighbor, bicubic interpolation, Enhanced Super-resolution GAN (ESRGAN) and high resolution fields. Note the consistently higher value of PSNR of the ESRGAN generate field in comparison to the bicubic interpolation

where MAX_1 is the maximum possible wind magnitude. It can be clearly seen the GANs has consistently higher $PSNR$ compared to the bicubic interpolation.

Fig. 5 presents the L2 norm computed from the high resolution wind field and the reconstructed fields using bicubic interpolation and GANs for 1800 datasets. One can see that the bicubic interpolation results in significantly greater errors which is in agreement with the observation from the Fig. 4.

As a matter of fact, bicubic interpolation improves the resolution exclusively based on its own contents, thus information lost from the downsampling phase is never recovered. GANs on the other hand learns the features of the wind flow and utilizes that information to recover the loss during the downsampling phase.

6. Conclusion and future work

The present work demonstrated a GANs based approach to super-resolution reconstruction from coarse scale wind field. We highlight the major findings from the work below:

- The GANs used in this work learned the important characteristics and features of the wind flow in complex terrain without the aid of any equation or explicit programming of the physics.
- GANs utilized the learned knowledge of the wind characteristics to reconstruct high resolution wind field from previously unseen coarse data.
- The GANs convincingly outperformed the bicubic interpolation technique that can generally be used for this purpose.
- Although the training of the GANs requires hyperparameter tuning and can be computationally very demanding, once the model is trained it can achieve a speed up of $10000\times$ when compared to generating the same high resolution field using a numerical simulator

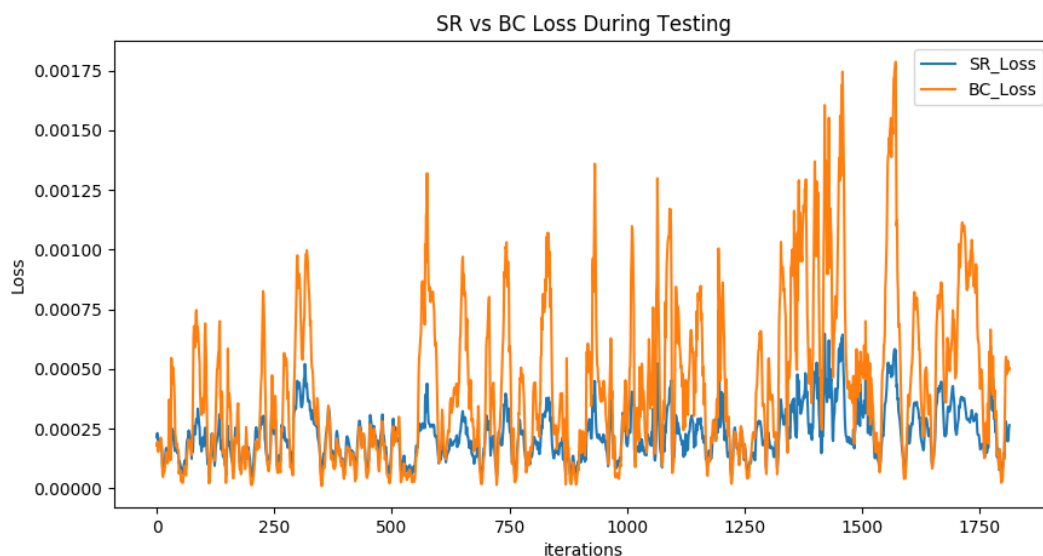


Figure 5. $\times 4$ enhancement: L2-norm error comparison of super-resolution (SR) and bicubic interpolation (BC) over part of the test set. The samples are recent, and were taken from the period September-October 2019. Each iteration corresponds to one hour.

In the current work we demonstrated the strength of combining physics based simulator with machine learning on 2D data set due to computational constraints. An extension to 3D is straight forward. At the moment the GANs were trained without the injection of any constraints or domain expertise for e.g. it can be interesting to evaluate how much the algorithm will get sensitized to the terrain information if provided during the training phase.

Acknowledgement

The authors acknowledge the financial support from the Norwegian Research Council and the industrial partners of the OPWIND: Operational Control for Wind Power Plants project (Grant No.: 268044/E20).

References

- [1] Rasheed, A., San, O., and Kvamsdal, T., 2020: Digital Twin: Values, Challenges and Enablers From a Modeling Perspective, *IEEE Access*, 8:21980–22012.
- [2] Siddiqui, M. S., Rasheed, A., Tabib, A., and Kvamsdal, T., 2019: Numerical investigation of modeling frameworks and geometric approximations on NREL 5MW wind turbine, *Renewable Energy*. 132, 1058–1075.
- [3] Seity, Y., P. Brousseau, S. Malardel, G. Hello, P. Bénard, F. Bouttier, C. Lac, and V. Masson, 2011: The AROME-France Convective-Scale Operational Model. *Mon. Wea. Rev.*, 139, 976–991
- [4] Utnes, T. and Eidsvik, K. J., 1997: Turbulent Flows over Mountainous Terrain Modelled by the Reynolds Equations. *Boundary-Layer Meteorology*. 79, 393–416.
- [5] Eidsvik, K. J., 2005: A System for Wind Power Estimation in Mountainous Terrain. *Prediction of Askervein Hill Data*, *Wind Energy*. Pages 237–249.
- [6] Rasheed, A., S¸ild, J. K., and Kvamsdal, T., 2014: A Multiscale Wind and Power Forecast System for Wind Farms, *Energy Procedia*. 53: 290–299.
- [7] Rasheed, A., Tabib, M. and Kristiansen, J., Wind Farm Modeling in a Realistic Environment Using a Multiscale Approach, Volume 10: *Ocean Renewable Energy of International Conference on Offshore Mechanics and Arctic Engineering*, 06 2017. V010T09A051.
- [8] Goodfellow, I.J., Pouget-Abadie, J., Mirza, M., Xu, B., Warde-Farley, D., Ozair, S., Courville, A.C., & Bengio, Y. (2014). *Generative Adversarial Networks*. ArXiv, abs/1406.2661.
- [9] Johnson, J., Alexandre, A., and Li, F.F. "Perceptual Losses for Real-Time Style Transfer and Super-Resolution." *Lecture Notes in Computer Science* (2016): 694–711. Crossref. Web.
- [10] Simonyan, K. and Zisserman, A., Very Deep Convolutional Networks for Large-Scale Image Recognition. Arxiv, arXiv:1409.1556
- [11] Wang, X., Yu, K., Wu, S., Gu, J., Liu, Y., Dong, C., Qiao, Y., and Loy, C.C. Esrgan: Enhanced super-resolution generative adversarial networks. In *The European Conference on Computer Vision Workshops (ECCVW)*, September 2018.

Appendix A: More qualitative comparison

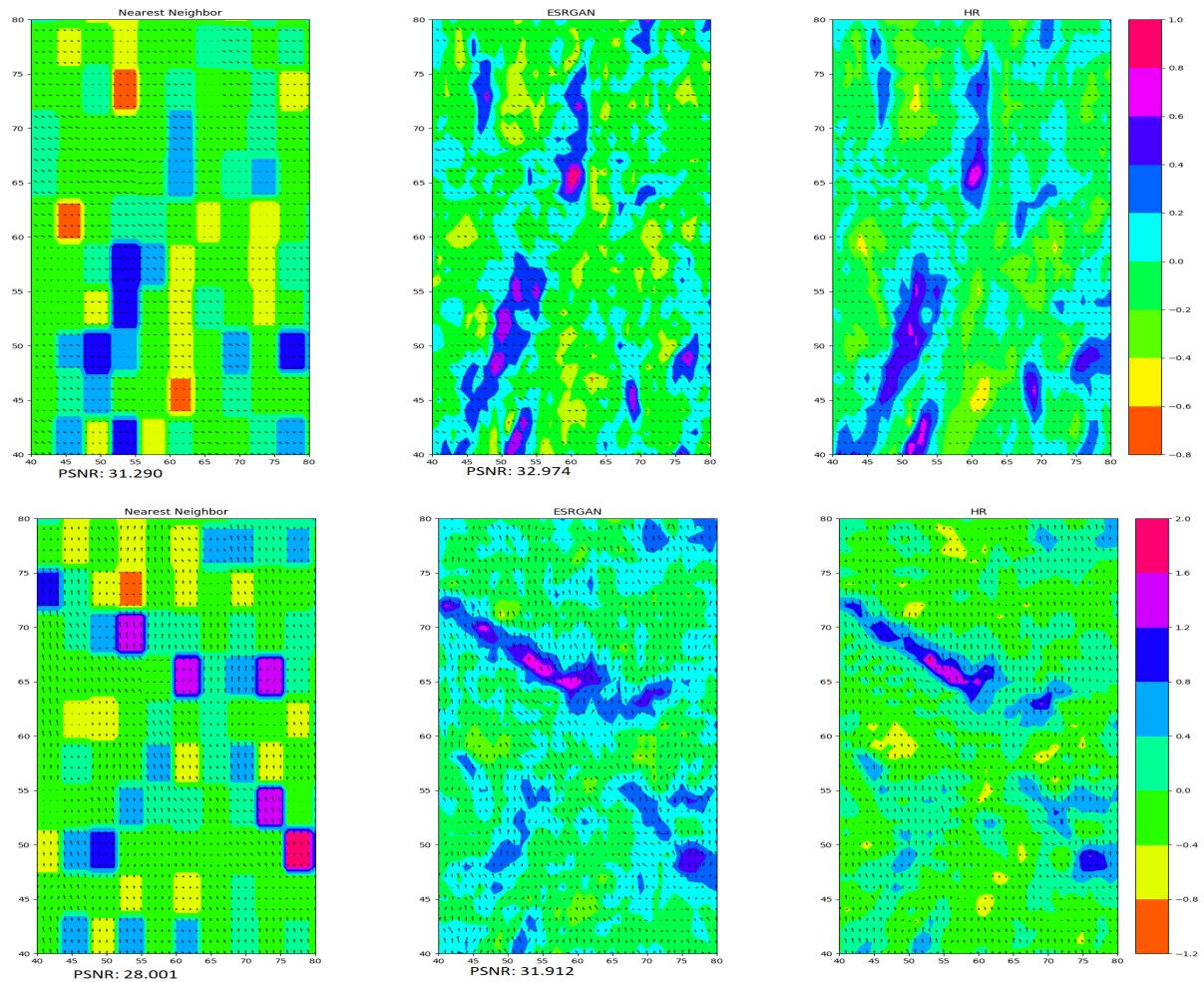


Figure 6. More zoomed in $(40 \times 40) \times 4$ enhancement qualitative results (from left to right) of the nearest neighbor, ESRGAN and high resolution fields.

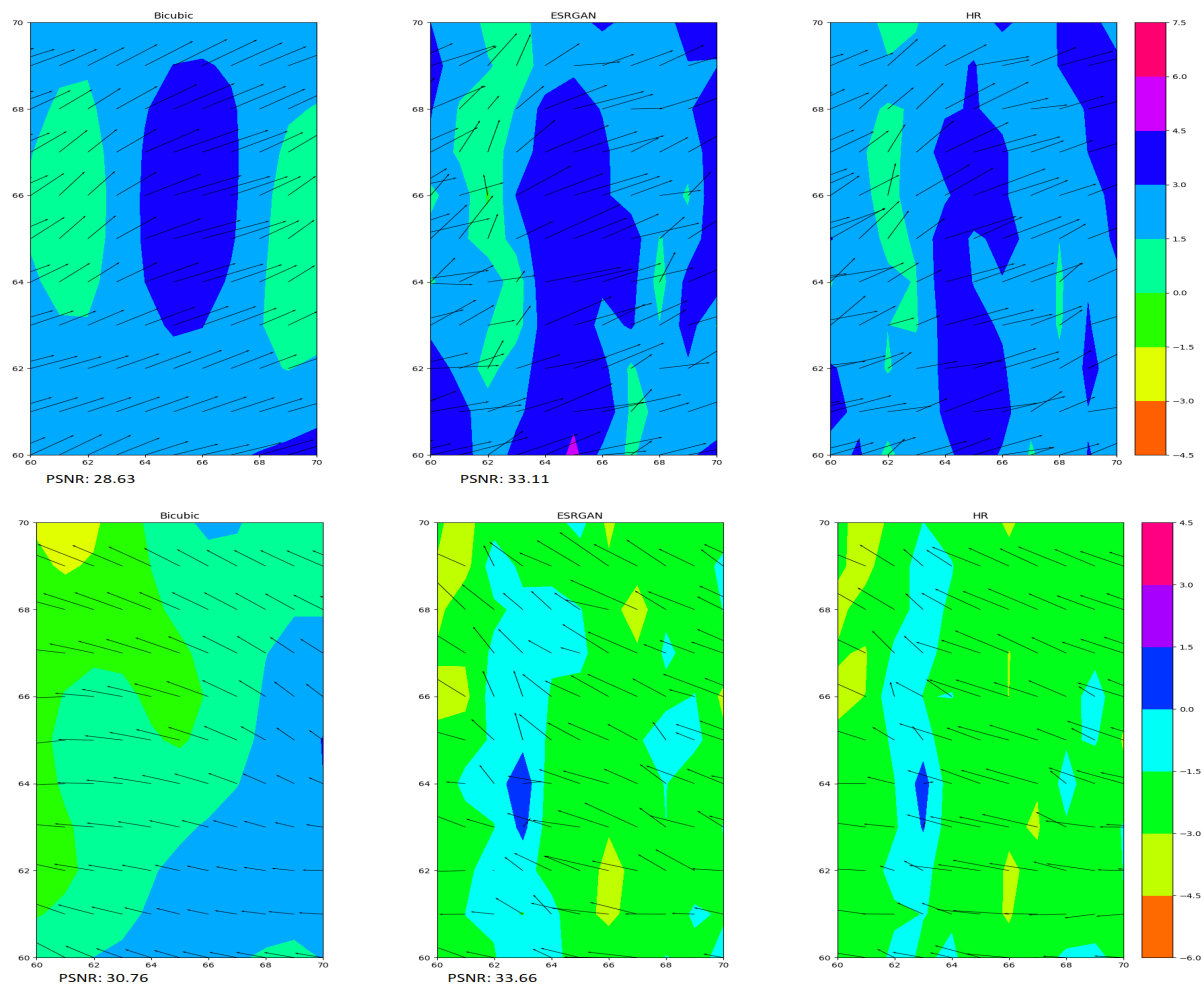


Figure 7. More zoomed in $(10 \times 10) \times 4$ enhancement qualitative results (from left to right) of the bicubic interpolation, ESRGAN and high resolution fields.